

Electronic supplementary information

Opening ZnSe/C Nanocages: Multi-Hierarchy Stress-Buffered Effect

Boosts Cycling Stability in Potassium-Ion Batteries

Jianhua Chu,^{‡a} Wei (Alex) Wang,^{‡b} Qiyao Yu,^{*c} Cheng-Yen Lao,^d Lin Zhang,^e Kai Xi,^d Kun Han,^a
Lidong Xing,^a Lei Song,^a Min Wang,^{*a} and Yanping Bao^a

^a *State Key Laboratory of Advanced Metallurgy, University of Science and Technology Beijing, Beijing 100083, China*

^b *Beijing Key Laboratory of Bio-inspired Energy Materials and Devices, School of Space and Environment, Beihang University, Beijing 100191, China*

^c *Institute of Advanced Structure Technology, Beijing Institute of Technology, Beijing 100081, China*

^d *Department of Materials Science and Metallurgy, University of Cambridge, Cambridge CB3 0FS, UK*

^e *Media Lab, Massachusetts Institute of Technology, Cambridge MA 02139, USA*

[‡] *These authors contributed equally to this work.*

^{*}*To whom correspondence should be addressed. Email: qiyaoyu@bit.edu.cn; worldmind@163.com*

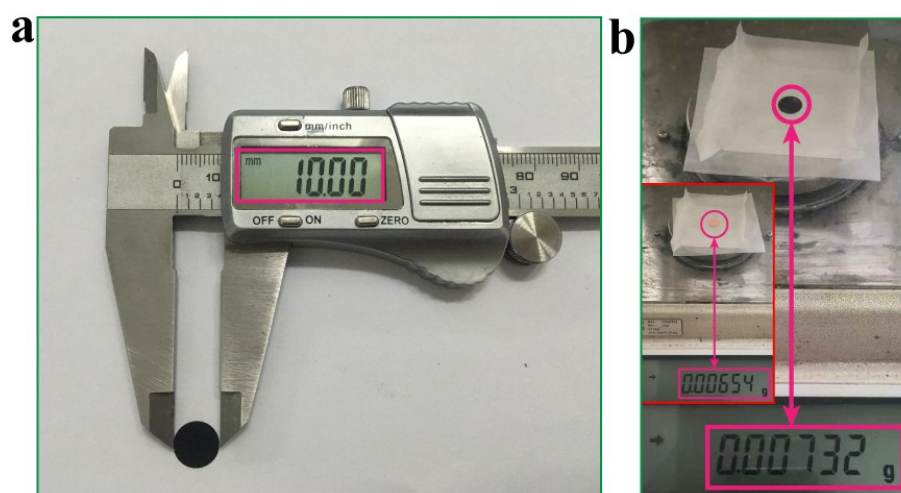


Fig. S1 Digital photographs show (a) the diameter (10 mm) and (b) the mass loading of the electrode.

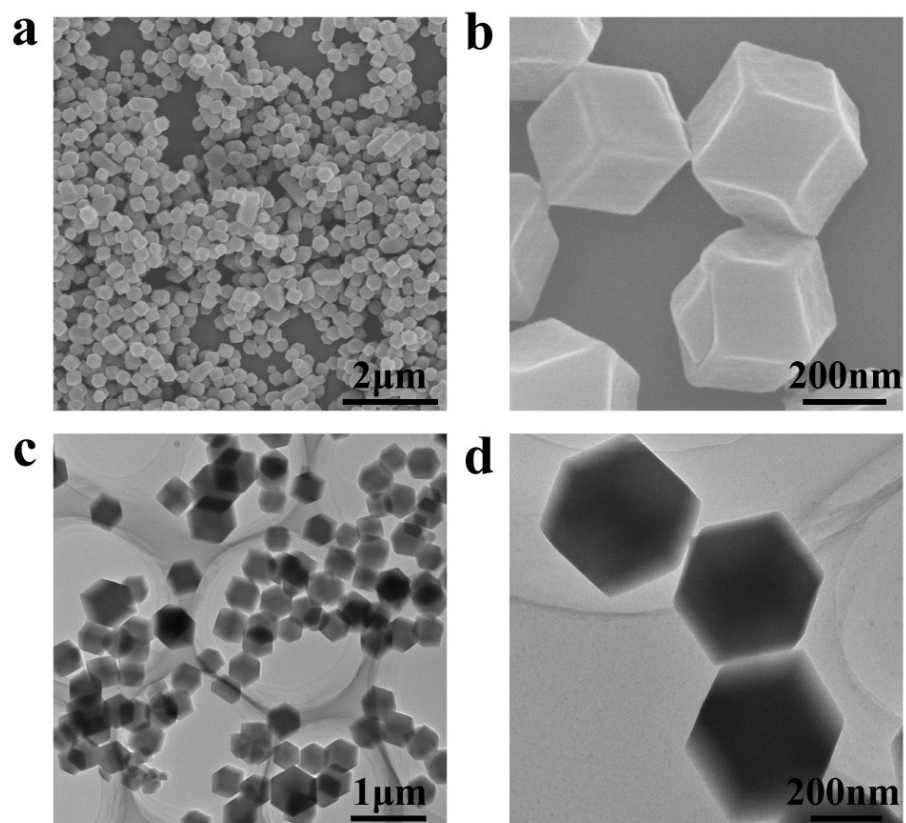


Fig. S2 Morphological and structural characterizations of ZIF8. (a, b) FESEM images and (c, d) TEM images of the ZIF-8.

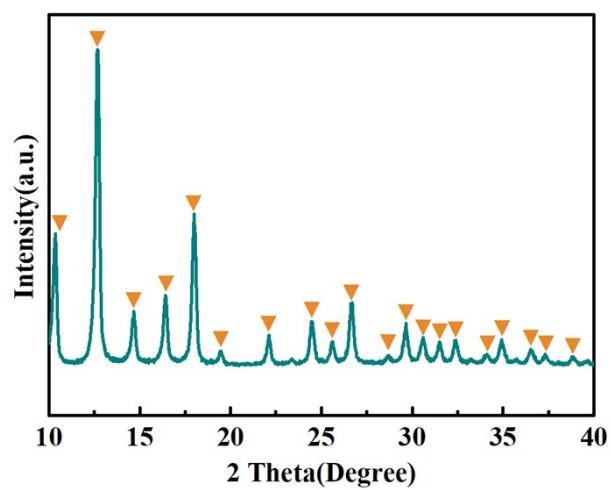


Fig. S3 Crystalline structural analysis of ZIF-8. The XRD pattern of the ZIF-8.

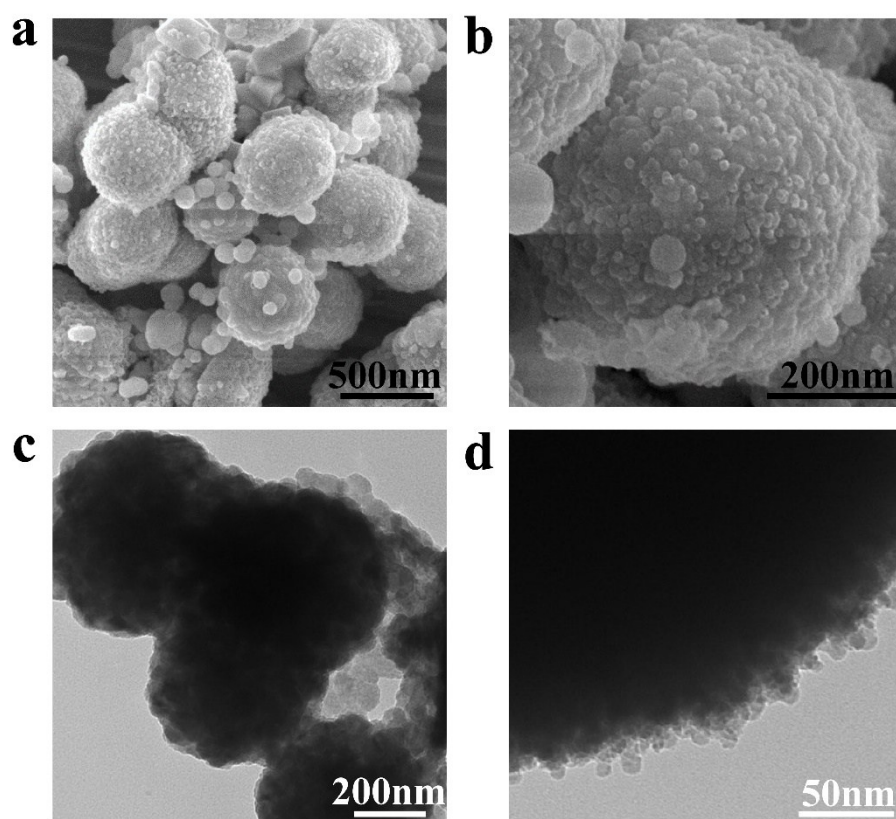


Fig. S4 Morphological and structural characterizations of ZnSe LS/C. (a,b) FESEM images and (c, d) TEM images of the ZnSe LS/C.

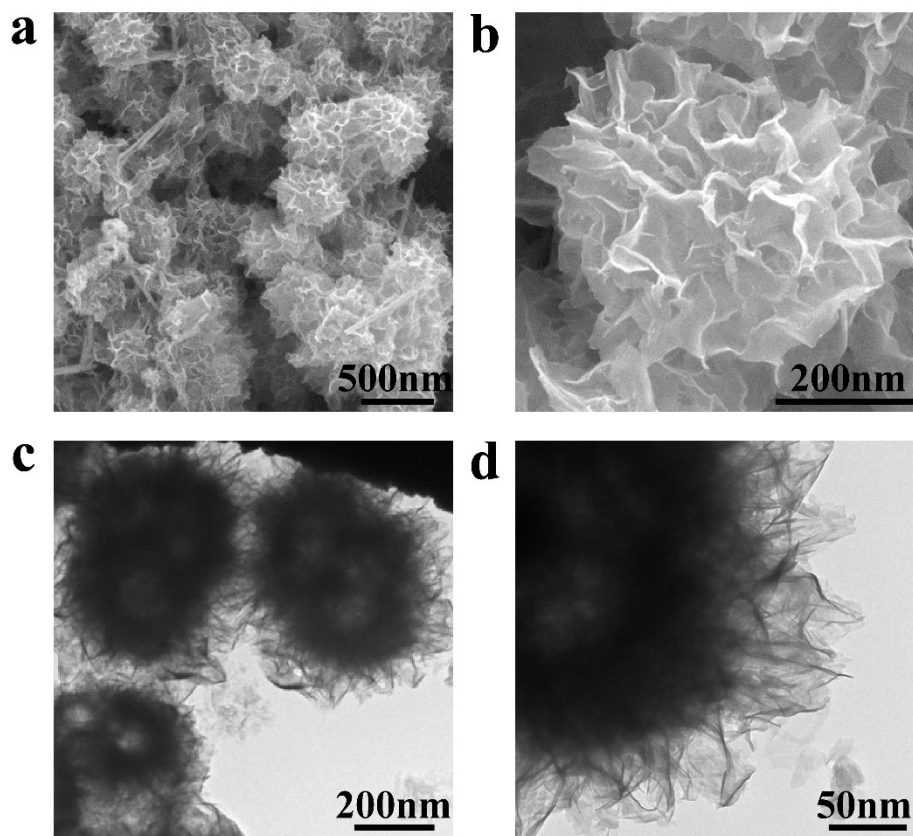


Fig. S5 Morphological and structural characterizations of ZnSe FS/C. (a, b) FESEM images and (c, d) TEM images of the ZnSe FS/C.

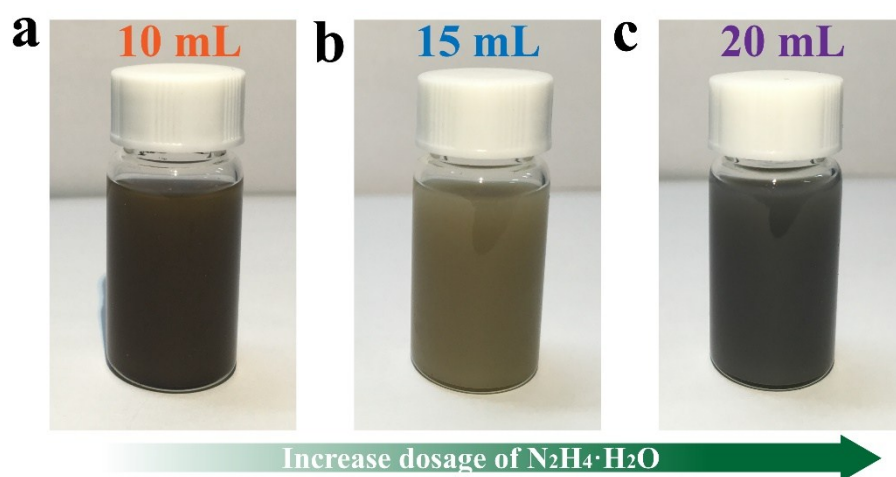


Fig. S6 Optical images of the ZnSe LS/C, ZnSe CS/C and ZnSe FS/C. Solution photograph of the (a) ZnSe LS/C, (b) ZnSe CS/C and (c) ZnSe FS/C with different the dosage of $\text{N}_2\text{H}_4 \cdot \text{H}_2\text{O}$.

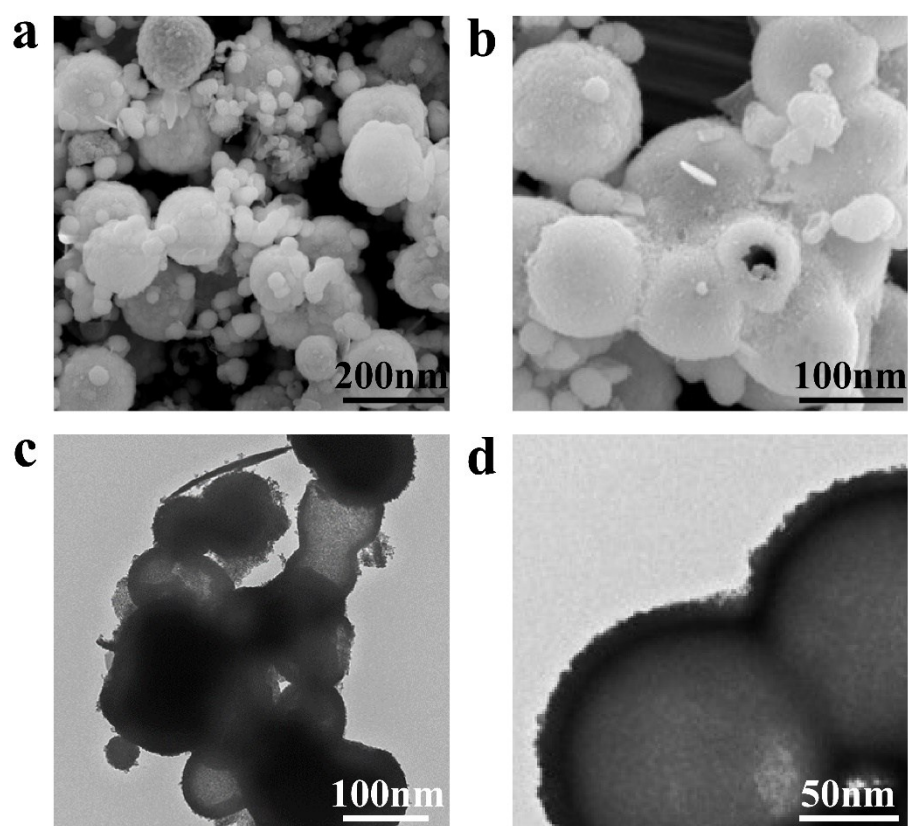


Fig. S7 Morphological and structural characterizations of ZnSe CS/C-0.5. (a, b) FESEM images and (c, d) TEM images of the hydrothermal holding time of 0.5 hours (ZnSe CS/C-0.5).

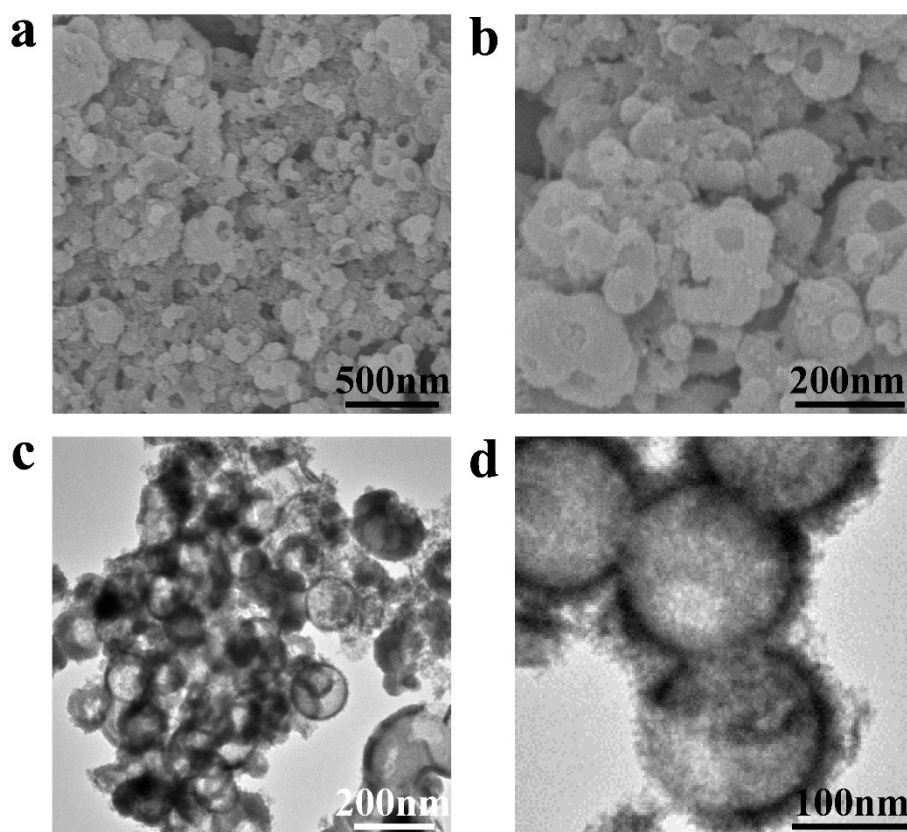


Fig. S8 Morphological and structural characterizations of ZnSe CS/C-2. (a, b) FESEM images and (c, d) TEM images of the hydrothermal holding time of 2 hours (ZnSe CS/C-2).

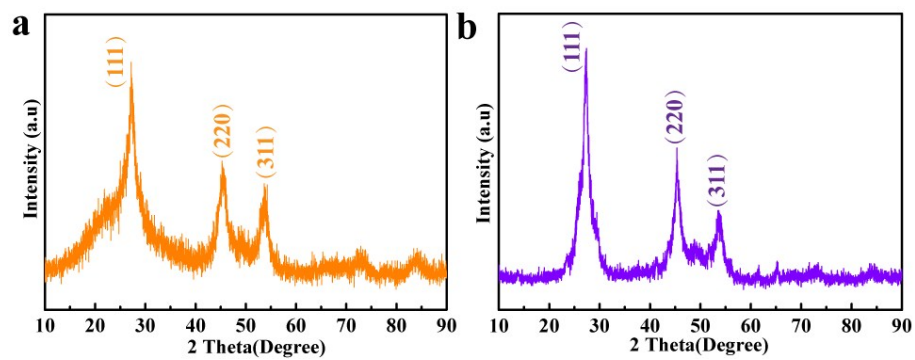


Fig. S9 Crystalline structural analysis of ZnSe LS/C and ZnSe FS/C. The XRD pattern of the (a) ZnSe LS/C and (b) ZnSe FS/C.

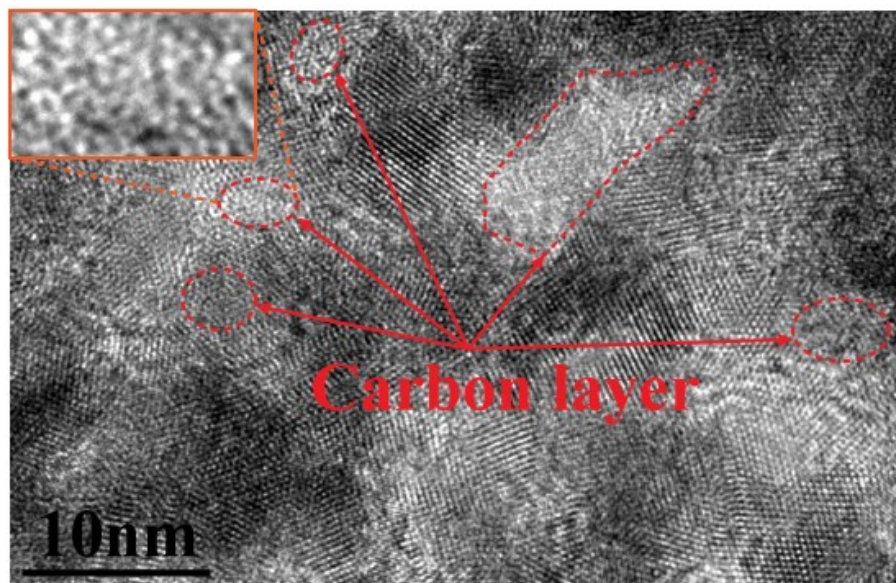


Fig. S10 Structural characterizations of ZnSe CS/C. The HR-TEM image of the ZnSe CS/C.

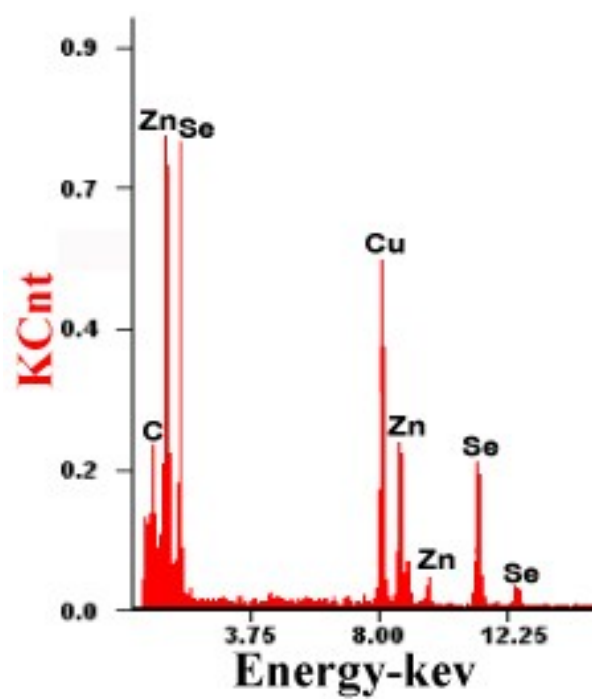


Fig. S11 Elemental analysis of ZnSe CS/C. The EDS spectrum of the ZnSe CS/C.

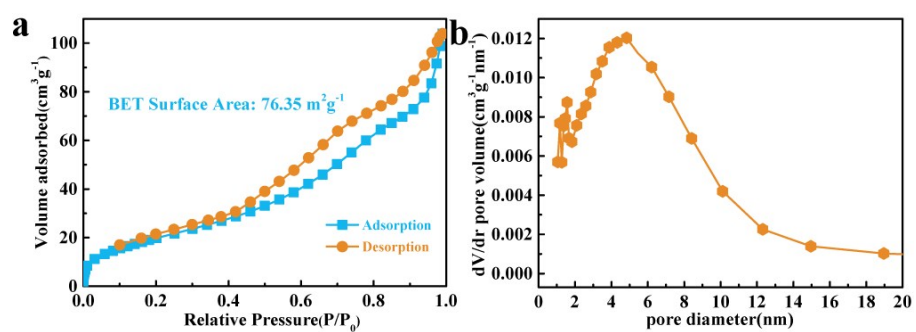


Fig. S12 (a) N_2 adsorption/ desorption isotherms and (b) corresponding pore size distribution of ZnSe LS/C.

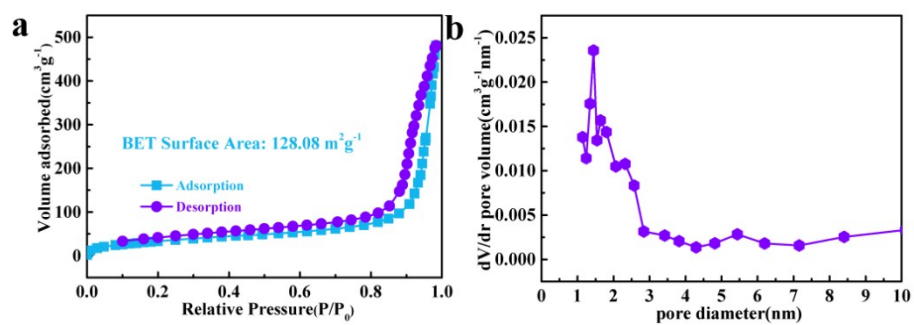


Fig. S13 (a) N_2 adsorption/ desorption isotherms and (b) corresponding pore size distribution of ZnSe FS/C.

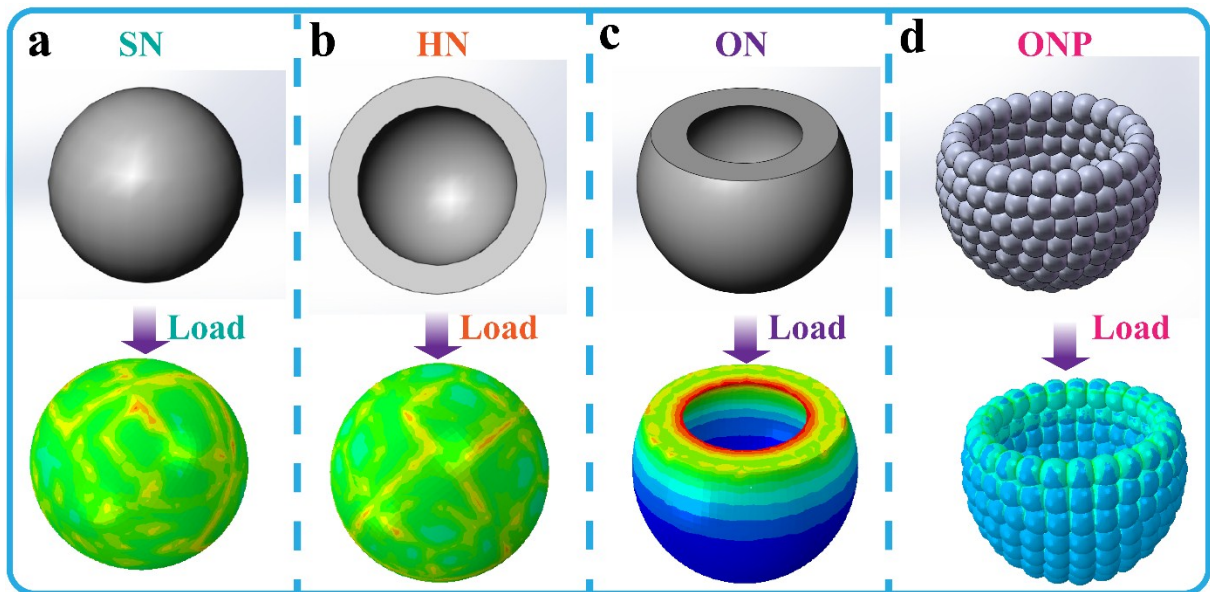


Fig. S14 Simulation of differential models structural stability suffer from diffusion-induced stresses. Drawing standard size models with Solidworks and calculated stress distributions overall view of (a) SN, (b) HN, (c) ON and (d) ONP.

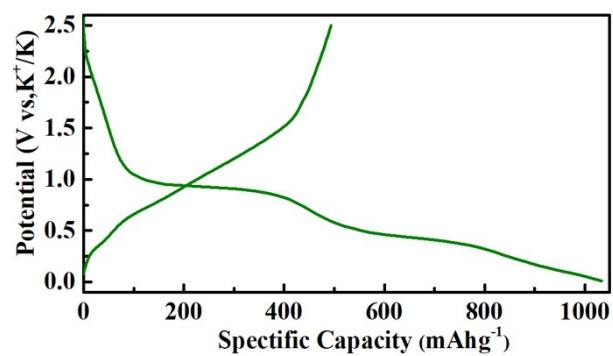


Fig. S16 The initial discharge/charge profiles analysis of ZnSe CS/C. The initial charge and discharge profiles of the ZnSe CS/C at 50 mA g⁻¹.

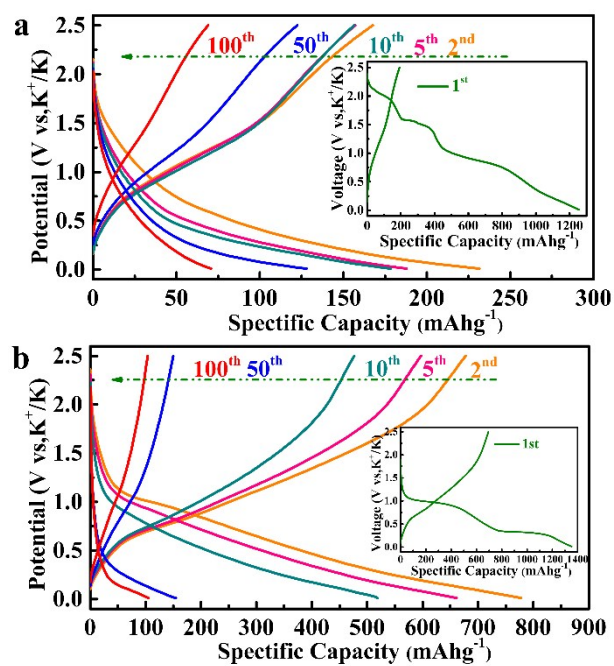


Fig. S17 Discharge/charge profiles analysis of the ZnSe LS/C and ZnSe FS/C for different cycles. Discharge/charge profiles for the 1st, 2nd, 5th, 10th, 50th and 100th cycles of (a) ZnSe LS/C and (b) ZnSe FS/C at 50 mA g⁻¹.

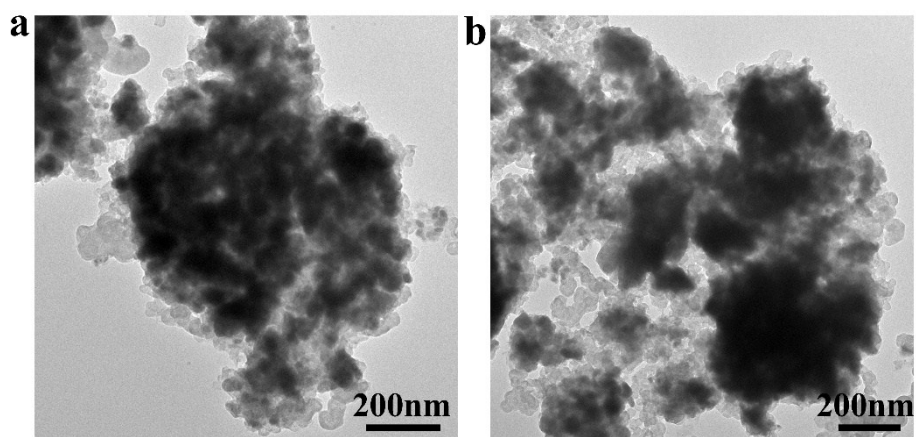


Fig. S18 TEM images of (a) ZnSe LS/C and (b) ZnSe FS/C electrode after 100 cycles at 100 mA g^{-1} .

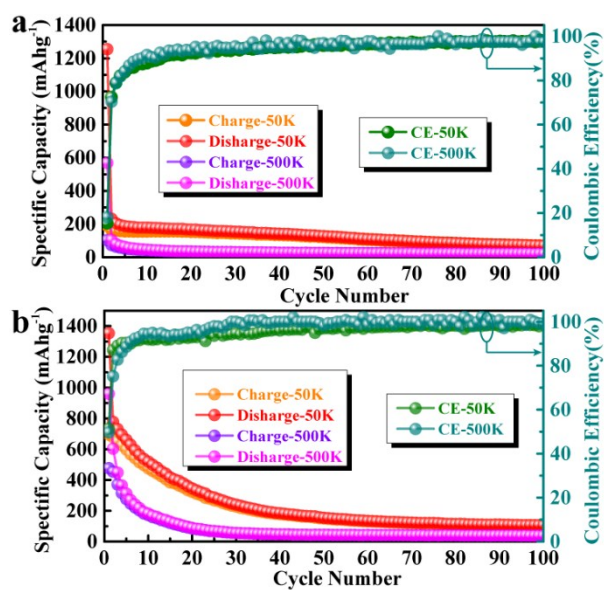


Fig. S19 Cycling performance analysis of the ZnSe LS/C and ZnSe FS/C. Cycling performance of (a) ZnSe LS/C and (b) ZnSe FS/C at 50 mA g⁻¹ and 500 mA g⁻¹, respectively.

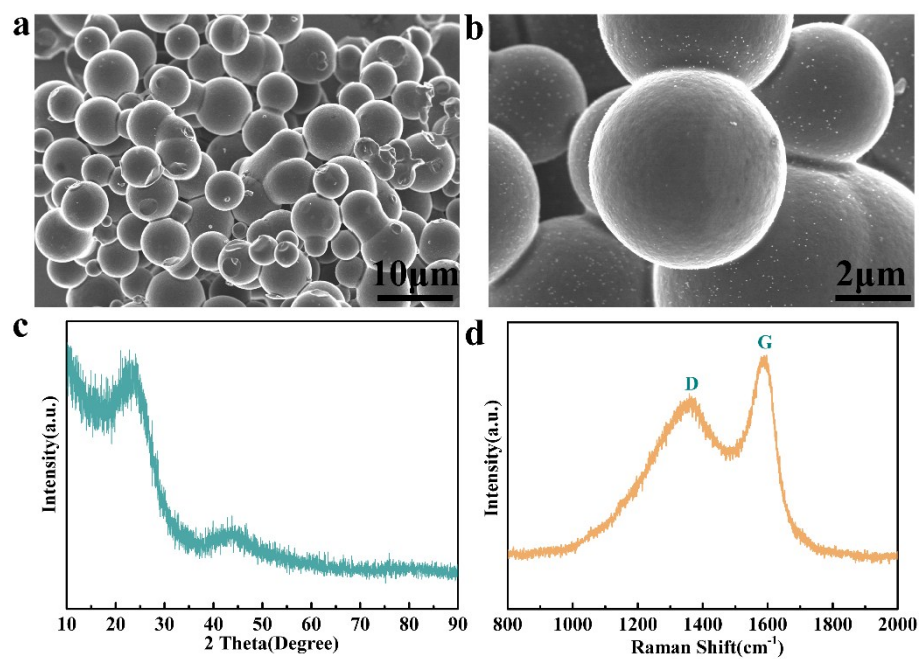


Fig. S20 (a, b) SEM images, (c) XRD pattern and (d) Raman spectrum of the as-prepared amorphous carbon.

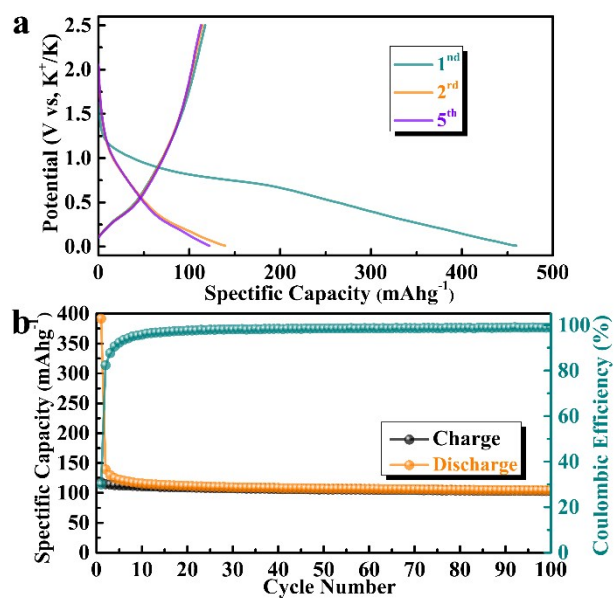


Fig. S21 Cycling stability and Coulombic efficiency of the amorphous carbon at 50 mA g⁻¹.

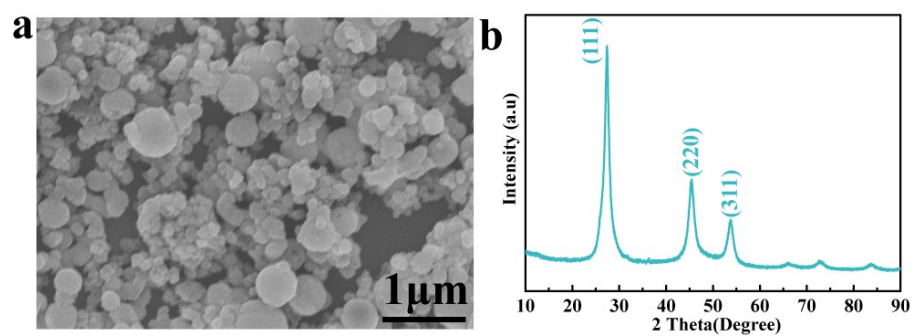


Fig. S22 (a) FESEM image and (b)XRD pattern of the as-prepared pure ZnSe.

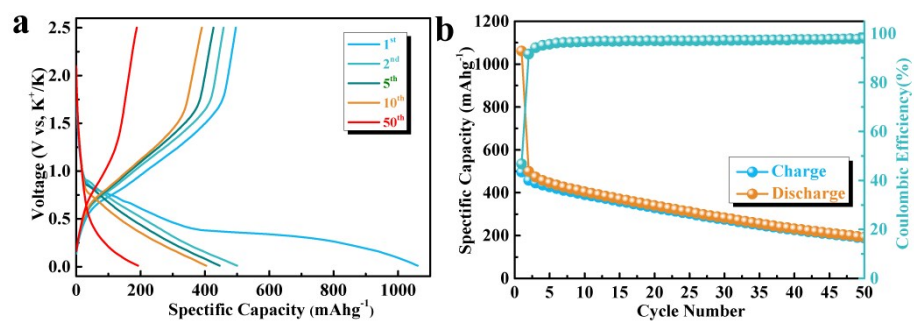


Fig. S23 (a) Charge–discharge voltage profiles from the first to fiftith cycle and (b) charge/discharge capacity of pure ZnSe at 50 mA g⁻¹.

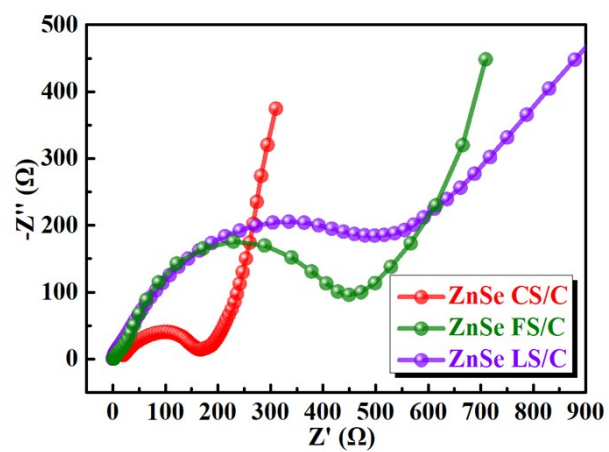


Fig. S24 Nyquist plots for ZnSe CS/C, ZnSe LS/C and ZnSe FS/C in original cycles, respectively.

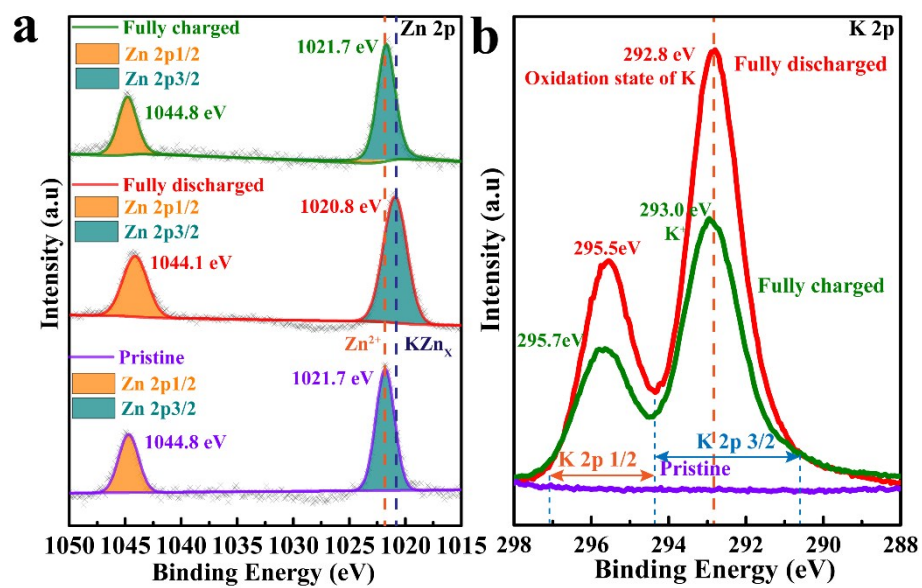


Fig. S25 *Ex situ* core-level XPS analysis for the ZnSe CS/C electrode at different potassiation/dopotassiation states. (a) Zn 2p and (b) K 2p.

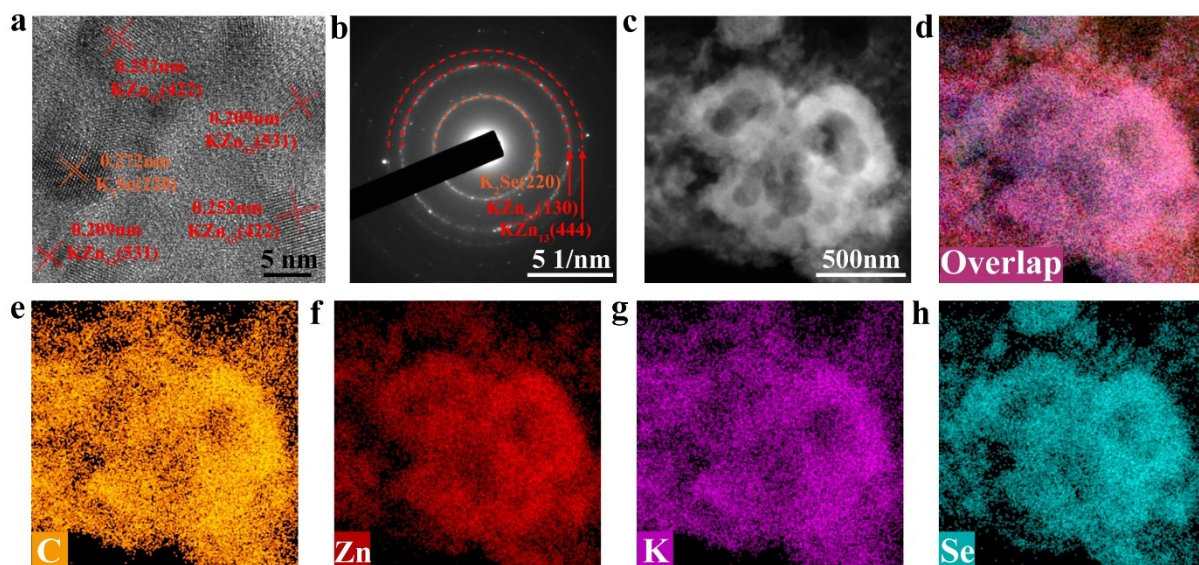


Fig. S26 (a) HRTEM image of the ZnSe CS/C electrode after fully discharged (0.01 V) and the corresponding (b) SAED patterns. (c) HAADF-STEM image and (d-h) EDS mappings of C, Zn, K, and Se in ZnSe CS/C electrode after fully discharged to 0.01 V.

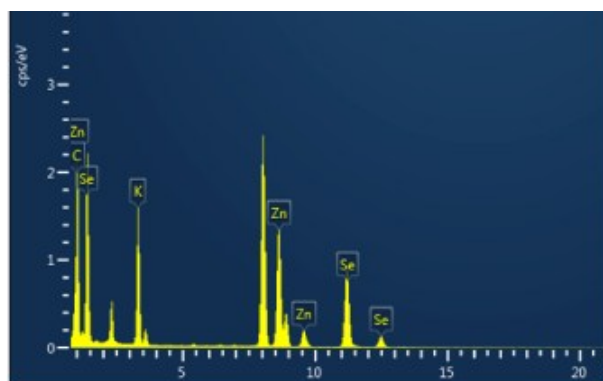


Fig. S27 The EDS spectrum of the ZnSe CS/C electrode after fully discharged to 0.01 V.

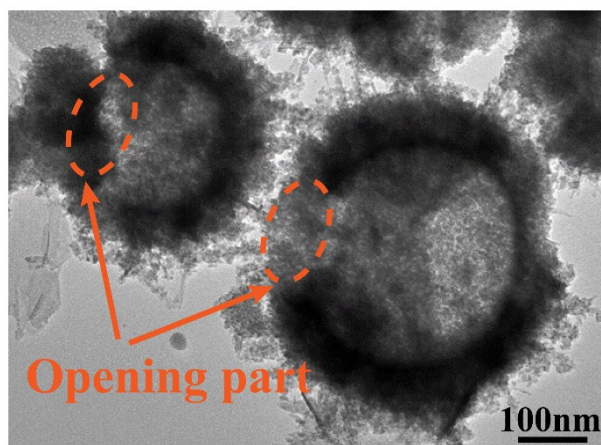


Fig. S28 Postmortem characterization of the ZnSe CS/C electrode after cycling. TEM image of ZnSe CS/C electrode after 100 cycles at 100 mA g⁻¹.

Table S1 The element content of the ZnSe CS/C via EDS mapping analysis.

Element	Weight %	Atomic %
Zn	52.58	23.95
Se	26.42	24.44
C	20.47	50.49
Totals	100.00	100.00

Table S2 The carbon sulfur analyzer data of ZnSe LS/C, ZnSe CS/C and ZnSe FS/C.

Sample	ZnSe LS/C	ZnSe CS/C	ZnSe FS/C
Carbon Content %	19.56	20.37	18.34

Table S3 The geometric size for various models.

Model	Outer diameter (nm)	Inner diameter (nm)	Radius of the particle sphere (nm)
I	75	---	---
II	75	55	---
III	75	55	---
IV	75	55	10

The opening portion is one quarter of the diameter direction of the entire sphere in model III and model IV.

Table S4 The element content of the ZnSe CS/C electrode after fully discharged to 0.01 V via EDS analysis.

Element	Weight %	Atomic %
Zn	23.71	12.74
Se	30.68	13.56
K	29.31	26.24
C	16.3	47.46
Totals	100.00	100.00